

Measurement of the D^0 , D^+ , and D_s^+ meson lifetimes

D. Averill, D. Blockus, B. Brabson, J.-M. Brom,* C. Jung,† H. Ogren, and D. R. Rust
Indiana University, Bloomington, Indiana 47405

M. Derrick, P. Kooijman,‡ J. S. Loos,§ B. Musgrave, L. E. Price,
J. Repond, and K. Sugano
Argonne National Laboratory, Argonne, Illinois 60439

B. Cork
Lawrence Berkeley Laboratory, Berkeley, California 94720

C. Akerlof, J. Chapman, D. Errede,** M. T. Ken, D. I. Meyer, H. Neal,
D. Nitz, R. Thun, and R. Tschirhart
The University of Michigan, Ann Arbor, Michigan 48109

S. Abachi, P. Baringer, B. G. Bylsma,†† R. DeBonte, D. Koltick, E. H. Low,‡‡
R. L. McIlwain, D. H. Miller, C. R. Ng, and E. I. Shibata
Purdue University, West Lafayette, Indiana 47907
(HRS Collaboration)
(Received 31 May 1988)

We report measurements of the lifetimes of the D^0 , D^+ , and D_s^+ (F^+) mesons produced in e^+e^- collisions at a center-of-mass energy of 29 GeV. The decay vertex distribution in the processes $D^0 \rightarrow K^-\pi^+$, $D^+ \rightarrow K^-\pi^+\pi^+$, and $D_s^+ \rightarrow \phi\pi^+$ were made using a vertex chamber installed in the High Resolution Spectrometer at the SLAC storage ring PEP. The measured lifetimes are $\tau_{D^0} = (4.4 \pm 1.0 \pm 0.6) \times 10^{-13}$ s, $\tau_{D^+} = (9.2^{+1.7}_{-1.3} \pm 1.6) \times 10^{-13}$ s, and $\tau_{D_s^+} = (3.1^{+2.4}_{-2.0} \pm 0.5) \times 10^{-13}$ s.

In addition the lifetime of the B^0 meson is determined assuming that only the B^0 and not the B^- decays to a D^{*+} meson. The B^0 is not directly observed. The lifetime τ_{B^0} is estimated indirectly to be $(8.2^{+5.7}_{-3.7} \pm 2.7) \times 10^{-13}$ s.

I. INTRODUCTION

The charm mesons have been a fruitful source of information regarding the interaction of quarks, primarily because the charm quark Q behaves as if it were almost independent of the lighter quark. The lifetime of charm mesons can be related to the lifetime of the charm quark if it is assumed that the lighter of the two quarks has only a minor influence on the decay process. In this so-called spectator model, illustrated in Fig. 1(a), the charm-quark lifetime can be related to the lifetime of the μ lepton, which decays in a similar way, by the equation

$$\tau_Q = \tau_\mu \left[\frac{m_\mu}{m_Q} \right]^5 B(Q \rightarrow e\nu_e X) \left[\sum_q |V_{qQ}|^2 \right]^{-1},$$

where V_{qQ} are the relevant Kobayashi-Maskawa matrix elements¹ and B is the semileptonic branching ratio. The extent to which this model is valid can be tested by comparing the lifetimes of the three charm mesons since the prediction of the model is that all charm mesons should have the same lifetime.

It is known, however, that the D^+ meson has a substantially longer lifetime than that of the D^0 or the D_s^+ meson. This difference might be due to the presence of

an additional W -exchange diagram that can contribute to the D^0 decay as shown in Fig. 1(b) as well as the annihilation diagram, shown in Fig. 1(c), which can contribute to the D_s^+ decay. Both of these diagrams are thought to be small since the decay of a pseudoscalar particle to two light fermions is suppressed by helicity conservation, as is well known for the decay $\pi^- \rightarrow e^- \nu_e$. Processes of this type are therefore probably not responsible for the entire difference in charm-meson lifetimes.

Another possible reason for the lifetime difference is that the D^+ , in contrast with the D^0 and D_s^+ , has the two decay channels shown in Fig. 2, which might interfere destructively since they lead to the same final state. This would result in a suppression of the D^+ decay rate so that $\tau_{D^+} > \tau_{D^0}$ as is observed.

Although a considerable number of charm-decay measurements have been made, the effects of the W -exchange diagrams are not fully understood.² Several theoretical analyses³ have been made, however, which go beyond the simple model outlined above and provide fairly good agreement with the data.

This paper describes the measurement of charm-meson lifetimes using data collected with the High Resolution Spectrometer (HRS) operated at the PEP storage ring located at the Stanford Linear Accelerator Center. A con-

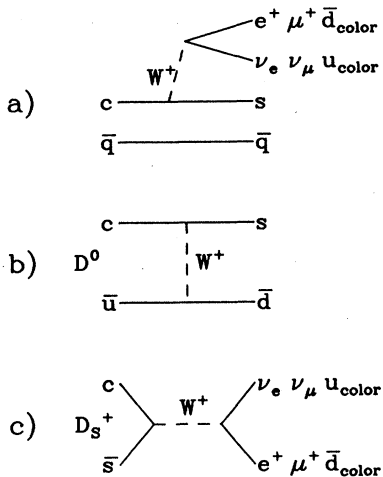


FIG. 1. (a) The weak-decay process for charm-meson decay. (b) The D^0 -exchange diagram. (c) The D_s^+ -annihilation diagram.

cise description of the lifetime measurement for the D_s^+ meson has already been published using a smaller event sample.⁴

The program of the HRS Collaboration to measure the charm-particle lifetimes began with the construction and installation of a high-precision tubular drift chamber in the space between the large central drift chamber and the beam pipe. Data were subsequently accumulated over the next 3 years of PEP running. The integrated luminosity which produced the sample of events used here was 200 pb^{-1} .

The same basic technique was used to measure the three charm-particle lifetimes. All of the events in the standard hadronic event sample were scanned for combinations of tracks that yielded the correct invariant mass for one of the charm mesons when a particular assignment of the K or π mass was used. At least two of the tracks were then fitted to a common intersection point. The distance of this vertex point from the known beam centroid together with the momentum of the reconstructed charm meson then yielded the proper decay time of

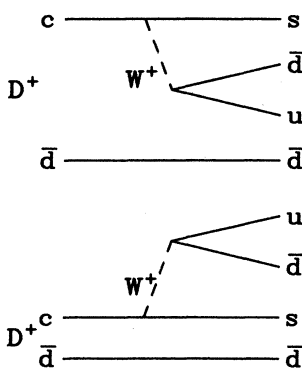


FIG. 2. The D^+ decay mode interference diagrams.

that particle. The distribution of decay times was decomposed into several components, of which one was the unknown lifetime of the charm meson.

This technique has been widely used at e^+e^- storage rings.^{5,2} There have also been measurements of charm-particle lifetimes by groups using fixed targets in external beam lines at CERN^{6,2} and Fermilab^{7,2} (especially E-691) and by bubble-chamber groups.^{8,2} The measurements reported in this paper possess similar systematic errors and confirm the observed lifetime differences between the mesons containing heavy quarks.

II. APPARATUS

The HRS detector has been described in general in a previous publication.⁹ There are also detailed descriptions of the central tracking drift chamber,¹⁰ of the vertex drift chamber,¹¹ and of the barrel shower counters.¹² In this section we review the features of the detector that are important for the lifetime measurements.

The outer drift chamber plus the two chambers mentioned above operated in a 1.62-T magnetic field. The outer drift chamber consisted of two layers of tubes at a radial distance of 2 m from the beam. The central drift chamber had 15 layers extending in radius from 0.2 m to 1.0 m and included eight stereo and seven axial layers. The vertex drift chamber had four layers of tubes between 0.091 m and 0.115 m in radial distance, an axial length which matched the acceptance of the central drift chamber, and an effective thickness of 0.4% of a radiation length.

The resolution of the outer and central chambers was $\sigma = 200 \mu\text{m}$ and the resolution of the vertex chamber was $\sigma = 100 \mu\text{m}$ per layer. The momentum resolution was found to be $\sigma_p/p^2 \approx 0.002 (\text{GeV}/c)^{-1}$ for high-momentum tracks. Such precision led to narrow mass peaks in the invariant-mass distributions for fully reconstructed decays and therefore to a relatively clean separation of the charm-particle signal from the background.

The extrapolation of the tracks to the interaction point was done to a precision of $120 \mu\text{m}$. This is sufficiently accurate to determine a vertex position in a typical charm-meson decay with an error which is of the same order as the distance from the beam centroid to the vertex position. The outer drift chambers, although contributing to the accuracy of the mass determination, were not used in the measurement of the vertex position because they contributed little to the final precision of that quantity but could possibly bias the vertex determination if there were a misalignment.

III. SELECTION OF EVENTS

We looked for candidate events in our standard sample of hadronic events corresponding to 200 pb^{-1} of integrated luminosity. These events were selected by requiring that there be at least five charged tracks in the event and that the sum of the charged and neutral energies be greater than 8 GeV. There are 44 000 of these events. In all of the following discussion reference to a charm particle includes the charge-conjugate partner.

A. $D^0 \rightarrow K^- + \pi^+$

The D^0 mesons were chosen to be daughters of D^{*+} mesons in the decay $D^{*+} \rightarrow D^0 + \pi^+$. There was no attempt to identify a track as a K or a π before calculating the mass. One track was chosen to be a K meson, another track of opposite sign was chosen as a π meson, and their invariant mass was calculated. The characteristic mass difference between the two charm mesons was then used to obtain a sample of D^0 mesons with nearly zero background. This mass difference, $\Delta = m_{D^{*+}} - m_{D^0}$, was calculated by taking another track with the same sign as the π meson from the D^0 decay as the D^{*+} decay product. The nominal value of Δ is $0.1454 \text{ GeV}/c^2$ (Ref. 13).

A separate analysis of the data was done for two regions of the variable z_{D^*} , which is the energy of the D^{*+} meson divided by 14.5 GeV , the energy of one of the beams. The data with $z_{D^*} \geq 0.4$ were used to find the lifetime of the D^0 meson. The data with $z_{D^*} < 0.4$, on the other hand, were used to extract a number for the lifetime of the B^0 meson under the assumption that B^0 -meson decays account for about half of the D^{*+} decays in this region of z_{D^*} (see Appendix C). Although this data sample is necessarily limited because the threshold for D^{*+} detection was at $z_{D^*} > 0.19$, the measurement of the B^0 lifetime is of interest.

The mass difference for both regions of z_{D^*} is presented in Fig. 3. In both histograms there is an enhancement corresponding to events with D^{*+} mesons. For these data an additional cut has been made on the absolute value of the cosine of the helicity angle of the decay kaon with respect to the D^0 direction in the D^0 rest frame, which serves to reduce the background from random track combinations. The data with $z_{D^*} < 0.4$ are more contaminated with background than the data with higher z_{D^*} because random combinations of tracks tend to form

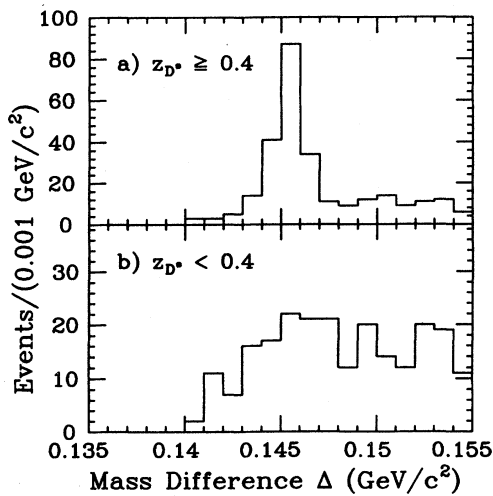


FIG. 3. The mass difference Δ between $K\pi$ combinations and the same combinations together with another π for $1.78 \leq M_{K\pi} \leq 2.05 \text{ GeV}/c^2$; (a) for $|\cos(\theta_K)^*| \leq 0.9$ and $z_{K\pi\pi} \geq 0.4$; (b) for $|\cos(\theta_K)^*| \leq 0.7$ and $z_{K\pi\pi} < 0.4$.

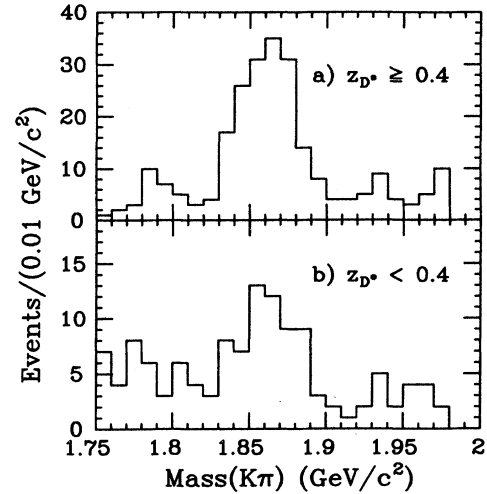


FIG. 4. The invariant mass in the range $1.75 \leq M_{K\pi} \leq 1.98 \text{ GeV}/c^2$ of the $K\pi$ combinations which have $0.143 \leq \Delta \leq 0.148 \text{ GeV}/c^2$; (a) for $|\cos(\theta_K)^*| \leq 0.9$ and $z_{D^*} \geq 0.4$; (b) for $|\cos(\theta_K)^*| \leq 0.7$ and $z_{D^*} < 0.4$.

false D^* mass values with low values of z_{D^*} . They have therefore been subjected to the selection $|\cos(\theta_K)^*| \leq 0.7$ as compared to $|\cos(\theta_K)^*| \leq 0.9$ for the data with higher z_{D^*} .

The invariant-mass distributions of the $K\pi$ combinations for those events where Δ is in the range $0.143 \leq \Delta \leq 0.148 \text{ GeV}/c^2$ are shown in Fig. 4.

B. $D^+ \rightarrow K^- + \pi^+ + \pi^+$

The decay mode, $D^{*+} \rightarrow D^+ + \pi^0$, which would have allowed a similar analysis as for the D^0 meson, was not available because our detector had a low efficiency for detecting the π^0 . Instead the D^+ was directly observed in the decay mode $D^+ \rightarrow K^- + \pi^+ + \pi^+$ ($B = 9.1\%$). The disadvantage was that by using a three-particle decay mode of the D^+ and not being able to use a mass difference cut with respect to the D^{*+} , the background was much higher than in the D^0 case. The invariant mass of the D^+ meson was calculated by taking one particle as a K meson and two particles with opposite sign to

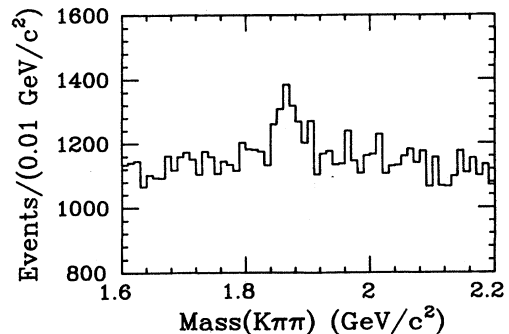


FIG. 5. The invariant mass of $K\pi\pi$ combinations with $z_{K\pi\pi} \geq 0.5$.

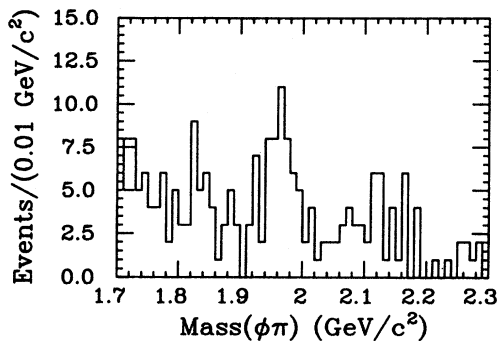


FIG. 6. The invariant mass of $\phi\pi$ events for $z_{\phi\pi} \geq 0.4$, $|\cos(\theta_K)^*| > 0.5$, and $|\cos(\theta_\phi)^*| < 0.9$.

the K meson as π mesons. The allowed range of z for the D^+ was chosen to be $z_{D^+} \geq 0.5$ in order to reduce the combinatorial background from low-momentum particles. The resulting invariant-mass distribution is shown in Fig. 5.

C. $D_s^+(F^+) \rightarrow \phi + \pi^+$

The sample of D_s^+ mesons was obtained by observing the decay mode $D_s^+ \rightarrow \phi + \pi^+$. The $\phi\pi$ mode was selected by first forming the K^+K^- combinations from all pairs of oppositely charged particles with momentum greater than 0.500 GeV/c and requiring the invariant mass to be between 1.0096 and 1.0296 GeV/c². To reduce the hadronic combinatorial background, a kinematic fit was performed on the track parameters of the two-kaon system subject to the constraint that $m_{KK} = 1.0196$ GeV/c². The events were kept if χ^2 was less than 50 in this fit. These ϕ candidates were then combined with all other charged particles, assuming a pion mass, and were required to have $z_{\phi\pi} > 0.4$. To enhance the signal-to-background ratio, decay angle cuts in the helicity frame that favor the decay of the spin-1 particle ϕ and the decay of the spin-0 particle D_s^+ were applied. The requirements were $|\cos(\theta_K)^*| > 0.5$, in the ϕ system and $|\cos(\theta_\phi)^*| < 0.9$ in the D_s^+ system. More details of the event-selection criteria can be found in a previous publication.⁴ The D_s^+ mass plot is shown in Fig. 6.

IV. VERTEX RECONSTRUCTION

The candidate charm-meson events were isolated as outlined above using information from the central and outer chambers. The tracks were then fitted to the primary vertex to obtain the best mass determination. Each of these events was then retracked using only information from the vertex and central chambers to obtain the best vertex information. In most events the tracks found in both reconstructions were identical and yielded the same invariant mass within the experimental resolution for the charm-particle combinations. These events were used for the lifetime analysis.

The next step was to constrain the tracks from the charm-meson decay vertex to come from a common

point. This was done with a least-squares fit using the track vectors and error matrices that are the output of the track-reconstruction step (not those resulting from the fit to the primary vertex). The method used is slightly different for the three charm mesons. For $D^0 \rightarrow K^- \pi^+$ there are only two tracks. In the case of the D^+ there are three tracks and all three are used to find the vertex. For the D_s^+ the π from the decay of the D_s^+ plus one of the kaons from the ϕ decay were used.

The fit was done effectively in two dimensions because the resolution in z (along the beam direction) was much worse than in the radial directions x and y . The method for removing the z dependence from the fit was to increase the error on the z -dependent terms entering into the track error matrices by a factor of 5. The number of constraints in the two-track fit is then essentially zero while in the three-track fit there is essentially one constraint.

A. D^0

Events within a mass range of $1.75 \leq M_{K\pi} \leq 2.00$ GeV/c² and within a Δ range of $0.135 \leq \Delta \leq 0.155$ GeV/c² were retracked using only the information from the vertex chamber and the central chamber. These wide cuts allowed us to include enough events to determine a background fraction and its apparent lifetime. A D^0 event, along with magnified details in the regions of the vertex chamber and the decay point, is shown in Fig. 7.

Events were rejected on the basis of the following criteria.

(i) The D^0 mass after retracking was not close enough to the known D^0 mass. A kinematic fit that varied the input track parameters to obtain the known mass of the D^0 was used and those events with large χ^2 were rejected. A cross comparison with the original fit was then made. Only those events originally within the range $1.83 \leq M_{K\pi} \leq 1.90$ GeV/c² were retained. The background events were not subjected to a secondary mass constraint but were required to be in the mass ranges in the original fit of $1.75 \leq M_{K\pi} \leq 1.80$ GeV/c² and $1.93 \leq M_{K\pi} \leq 2.00$ GeV/c².

(ii) The mass difference was not in the range $0.143 \leq \Delta \leq 0.148$ GeV/c².

(iii) One of the tracks from the D^0 shared one or more hits in the vertex chamber with any other track. These events were eliminated because hit sharing tends to bias the vertex position to a longer distance from the interaction point.

(iv) Fewer than a minimum number of hits in the vertex chamber were fit to the track. For $z_{D^0} \geq 0.4$ the minimum number was three while for $z_{D^0} < 0.4$ it was two.

The tracks from the surviving D^0 candidates were then refitted in the x - y plane subject to the constraint that they pass through a common point. This vertex was taken to be the decay vertex for the event. The distributions of vertex χ^2 are shown in Fig. 8. A few events are cut out at this stage because the χ^2 is abnormally large ($\chi^2 \geq 0.75$ for $z_{D^0} \geq 0.4$ or $\chi^2 \geq 0.5$ for $z_{D^0} < 0.4$). The vertex-

position error along the D^0 direction could sometimes be very large if, for instance, the opening angle was very small. These few anomalous events were removed by requiring that this error be less than 1.2 mm. The distributions of vertex-position errors are shown in Fig. 9.

After all these cuts were applied there remained 55 events with $z_{D^*} \geq 0.4$ and 22 events with $z_{D^*} < 0.4$ that were used to obtain the D^0 lifetime. The invariant-mass plots of these events, together with the background events which passed the same cuts, are shown in Fig. 10.

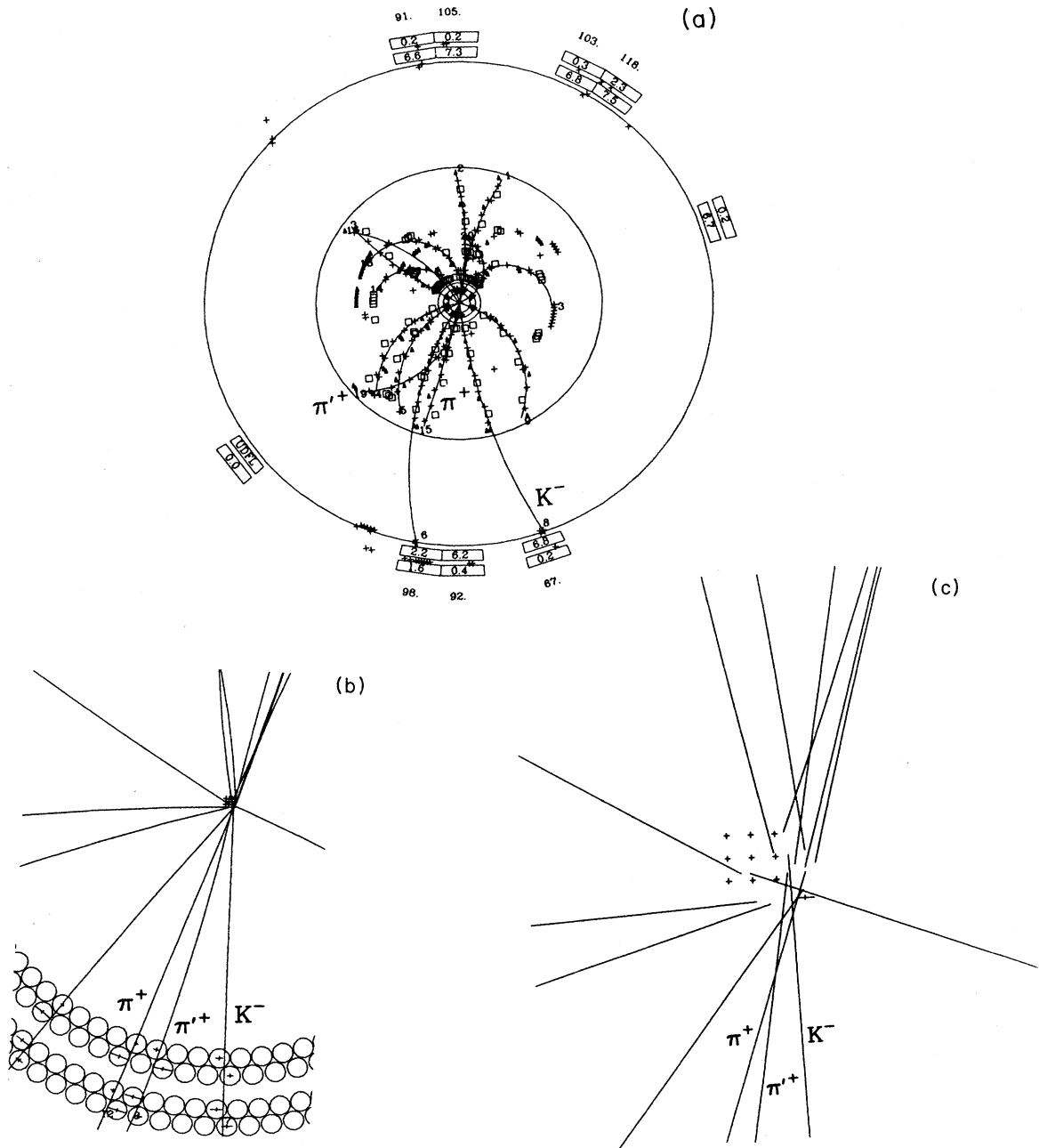


FIG. 7. A typical D^0 event in the HRS. (a) The axial view of all the detector components showing all of the hits in the drift chambers and the barrel shower counters. The lower jet contains the reconstructed $D^0 \rightarrow K^- \pi^+$ decay. This reconstruction included the outer chamber but not the vertex chamber. The K^- and π^+ tracks are identified as such and the π^+ from the D^* decay is labeled π'^+ . (b) The relevant tracks in the vertex chamber reconstructed using the vertex chamber but not the outer chamber. The same labels are used as in (a). (c) The same tracks projected to the interaction region. The crosses form a 1-mm grid at the origin of the detector. The small cross just to the lower right of the origin shows the position and size of the beam for this run.

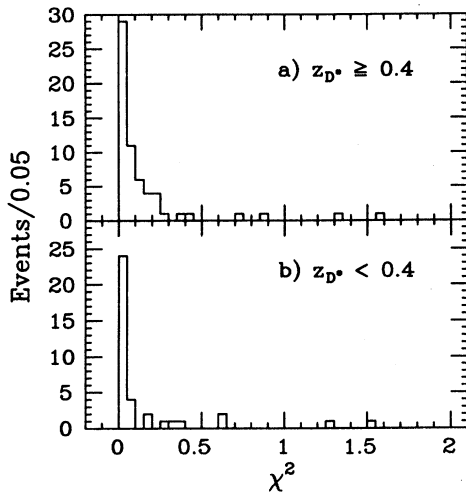


FIG. 8. The vertex χ^2 distribution for the fit of the two tracks of the D^0 decay for events passing the mass and track-quality cuts described in the text: (a) for $z_{D^*} \geq 0.4$; (b) for $z_{D^*} < 0.4$.

There are seven background events in the mass regions between 1.75 and 1.80 GeV/c^2 and 1.93 and 2.00 GeV/c^2 in the sample with $z_{D^*} \geq 0.4$. Thus we estimate a background contamination of $(7 \pm 4)\%$ in the accepted mass range of 1.83 to 1.90 GeV/c^2 . For the sample with $z_{D^*} < 0.4$ the number of background events in the mass regions between 1.70 and 1.79 GeV/c^2 and 1.93 and 2.05 GeV/c^2 is 17, giving a background contamination of $(19 \pm 5)\%$ in the accepted mass range from 1.83 to 1.88 GeV/c^2 .

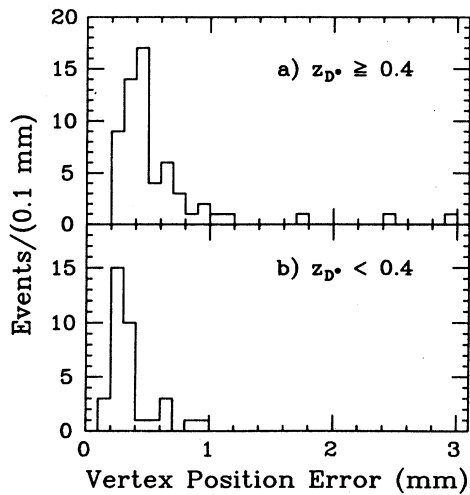


FIG. 9. The distribution of vertex-position error along the D^0 direction in the fit of the K and π tracks to a common vertex for events which pass the mass and track-quality cuts described in the text and the vertex χ^2 cut: (a) for the events with $z_{D^*} \geq 0.4$; (b) for the events with $z_{D^*} < 0.4$.

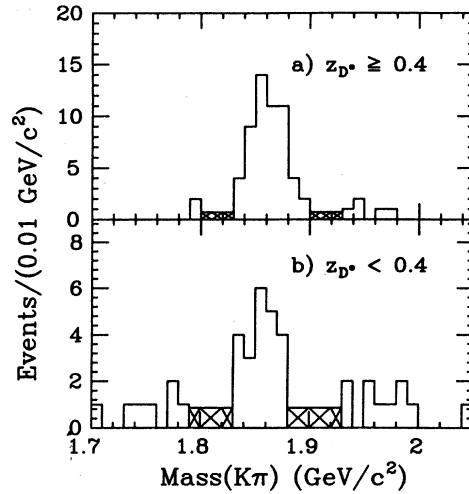


FIG. 10. The invariant-mass distribution for the events used to obtain the D^0 lifetime together with background events: (a) for $z_{D^*} \geq 0.4$; (b) for $z_{D^*} < 0.4$. The bins with \times 's show the estimated levels of background under the peaks.

B. D^+

After the D^+ events were selected, they were retracked using the vertex and central chambers to determine the best projection to the intersection region. At this point a series of cuts was imposed to guarantee high-quality tracks. Candidate $K\pi\pi$ tracks that shared a cell with any other track in any of the vertex chamber layers were removed, thus eliminating the entire event from the sample. This was done to avoid a systematic bias which could produce detached vertices and therefore a nonzero lifetime. The invariant-mass calculations for the two different tracking schemes were also required to agree within $\pm 40 \text{ MeV}/c^2$.

The vertex of the $K\pi\pi$ tracks was determined by a least-squares fit in two dimensions to a common point. Those decay vertices fitted with $\chi^2/\text{degrees of freedom (DF)} \geq 3.0$ and those which had a vertex-position error greater than 2.4 mm in the direction of the momentum of the D^+ were removed. The distributions of vertex χ^2 and position error are shown in Figs. 11 and 12, respectively.

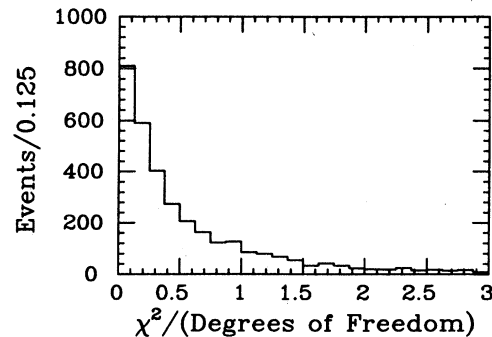


FIG. 11. The distribution of $\chi^2/(\text{degrees of freedom})$ for the fit to a common vertex of the $K\pi\pi$ tracks with $1.7 \leq M_{K\pi\pi} \leq 2.0 \text{ GeV}/c^2$.

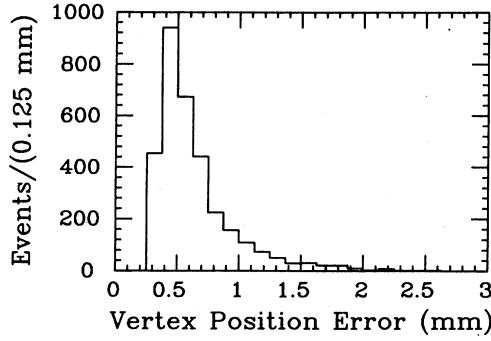


FIG. 12. The distribution of vertex position error along the D^+ direction in the fit to a common vertex of the $K\pi\pi$ tracks with $1.7 \leq M_{K\pi\pi} \leq 2.0 \text{ GeV}/c^2$.

The invariant-mass plot of the resulting sample is shown in Fig. 13. A fit to this mass distribution consisting of a Gaussian distribution and a linear background determined the number of D^+ events to be 155 above a background of 609 events in the mass region between 1.830 and 1.890 GeV/c^2 . The fitted D^+ mass was $1.858 \pm 0.015 \text{ GeV}/c^2$, consistent with the nominal value which is $1869.3 \text{ GeV}/c^2$ (Ref. 13).

C. D_s^+

Tracks used in the vertex fit were required to have at least three measured points in the vertex chamber layers and to have no shared hits in the vertex chamber. All three decay particle tracks could, in principle, be fitted to a common vertex position as was done in the case of the D^+ . The two K tracks, however, are nearly parallel and so do not locate a useful vertex by themselves. Each together with a pion could locate a vertex but the independent information in the two measurements is small. This small amount of additional precision must be balanced against the reduction of the event sample incurred by requiring three rather than two tracks with stringent quality criteria. It was found that it was better to use the π track and only one K track when determining the D_s^+ vertex position. Using only two tracks, with the criteria described above, reduced the event sample by 35%.

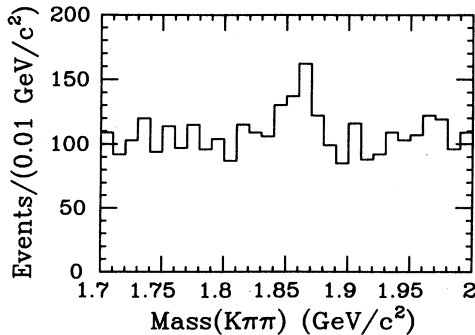


FIG. 13. The invariant-mass distribution for the $K\pi\pi$ combinations after all cuts have been made.

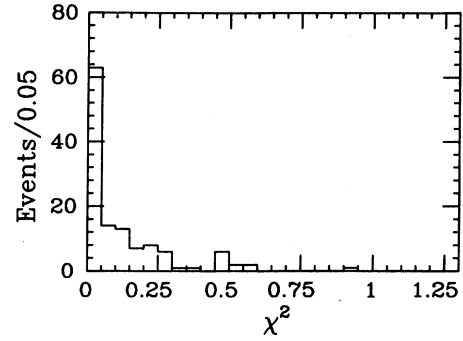


FIG. 14. The distribution of χ^2 for the fit of two of the tracks of the D_s^+ decay to a common vertex for events in the mass range $1.7 \leq M_{\phi\pi} \leq 2.3 \text{ GeV}/c^2$ after the track-sharing cuts have been made.

Another cut, which reduced the data sample by an additional 10%, was to require that the error in the fitted decay vertex position in the plane perpendicular to the beams be less than 1.2 mm along the D_s^+ flight direction. All events passed the criterion $\chi^2 \leq 1.0$. The relevant distributions are shown in Figs. 14 and 15. The final mass plot after all of these cuts is shown in Fig. 16.

This plot was divided into three different mass ranges—the lower hadronic combinatorial background region ($1.70 \leq M_{\phi\pi} \leq 1.91 \text{ GeV}/c^2$), the D_s^+ signal region ($1.94 \leq M_{\phi\pi} \leq 1.99 \text{ GeV}/c^2$), and the upper hadronic combinatorial background region ($2.02 \leq M_{\phi\pi} \leq 2.30 \text{ GeV}/c^2$). The 23 events observed in the D_s^+ region were used for the lifetime measurement. The estimated background in the signal region was 5 events.

V. BEAM POSITION AND ENVELOPE

It would have been desirable to use the information from the other tracks in the event to determine the primary event vertex. This could not be done in a satisfactory way, however, and instead the average beam position was measured for each set of events in a run corresponding to a storage ring fill cycle.

At PEP the ring was typically refilled every 1–2 h,

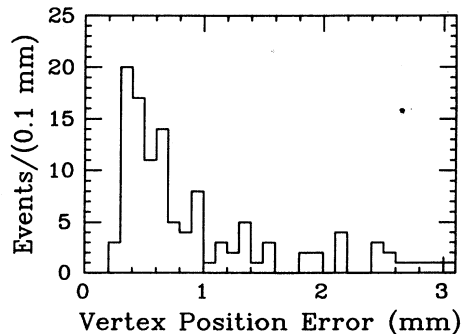


FIG. 15. The distribution of vertex position error for the fit of two of the tracks of the D_s^+ decay to a common vertex for events in the mass range $1.7 \leq M_{\phi\pi} \leq 2.3 \text{ GeV}/c^2$ after the shared hits cut has been made.

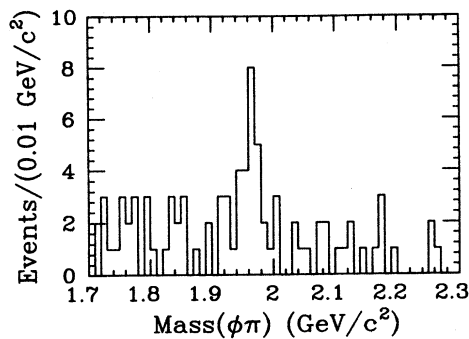


FIG. 16. The invariant-mass distribution of the $\phi\pi$ combinations after all cuts have been made.

yielding an integrated luminosity for the fill of approximately 100 nb^{-1} . In order to measure the mean-beam position it was necessary to select good quality tracks that did not originate from secondary vertex decays. A set of tracks from a series of Bhabha-scattering events satisfied these conditions. The Bhabha tracks may be considered as originating from the average beam position, which was consequently determined by fitting them to the same crossing point. Up to 20 Bhabha events were fitted as a group. Since about 60 Bhabha events are expected for 100 nb^{-1} of integrated luminosity, there were typically three such groups in a run. The final average beam position was determined by taking the average of the fitted values of these groups. The errors were typically $\pm 50 \mu\text{m}$ in x and $\pm 20 \mu\text{m}$ in y . The average beam positions determined by this method for the runs used for this analysis are shown in Figs. 17 and 18. Six Bhabha events in a run were required for an acceptable beam position measurement. If a run were so short that this condition was not satisfied, the average of the beam positions of the preceding and the succeeding runs was used. The z beam

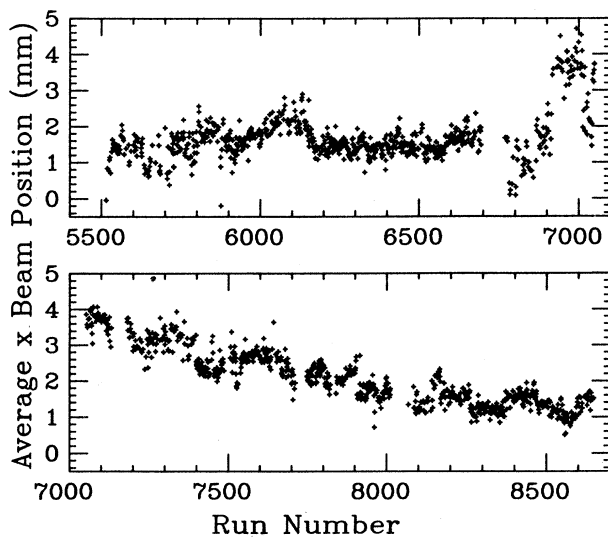


FIG. 17. The x average beam positions with respect to the detector axis for runs used in the measurement of the charm lifetimes. The error on each point is typically $\pm 50 \mu\text{m}$.

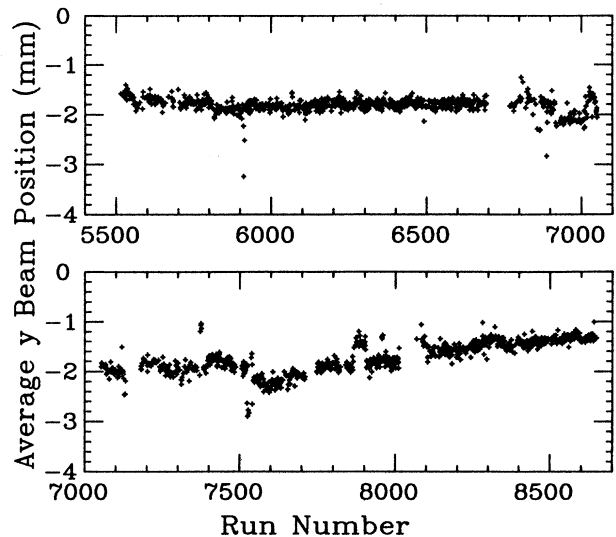


FIG. 18. The y average beam positions with respect to the detector axis for runs used in the measurement of the charm lifetimes. The error on each point is typically $\pm 20 \mu\text{m}$.

position was constrained to be zero in this fit since the vertex chamber does not provide any z information.

The PEP beam size is about $500 \mu\text{m}$ in x by $200 \mu\text{m}$ in y . The main contribution to the x beam size is the horizontal oscillation of the beams due to the synchrotron radiation. The same Bhabha-scattering events that were used to determine the beam positions were used to measure the beam size. The x and y dimensions of the beam can be obtained by measuring the impact-parameter distributions of the horizontal and the vertical tracks. The impact-parameter distributions of the tracks which make angles with the x or y axis of less than 0.1 rad are shown in Fig. 19. The standard deviations of these distributions, fitted by a Gaussian shape, were $395 \mu\text{m}$ in x and $140 \mu\text{m}$

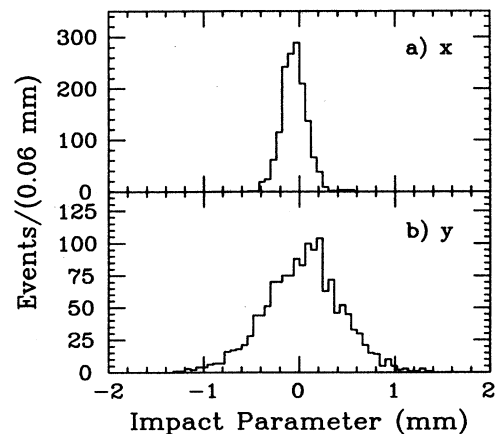


FIG. 19. The distributions of the x and y average impact parameters for tracks in Bhabha-scattering events which make angles of less than 0.1 rad with the x and y axes. The x impact parameter measures the width of the beam in the y dimension and vice versa.

in y . These widths are the sums of the true beam dimensions, the extrapolated Bhabha track errors ($\sigma = 102 \mu\text{m}$), and other systematic errors, including small excursions of the beam during a run. Removing the contribution of the track error, these plots determined the effective beam dimensions to be $\sigma_x = 383 \mu\text{m}$ and $\sigma_y = 98 \mu\text{m}$.

VI. FITTING THE LIFETIME DISTRIBUTION

The most probable decay distance in the plane perpendicular to the beams was calculated for each charm-particle candidate by using the expression¹⁴

$$l' = \frac{x_v V_{yy} u_x + y_v V_{xx} u_y - V_{xy}(x_v u_y + y_v u_x)}{V_{yy} u_x^2 + V_{xx} u_y^2 - 2V_{xy} u_x u_y},$$

where (x_v, y_v) is the decay vertex position relative to the average beam position, V_{ij} are the elements of the total variance matrix (the sum of the vertex-position and beam-position variance matrices), and u_i are the two-dimensional direction cosines of the decaying charm particle. The error on the most probable decay distance is given by¹⁴

$$\delta l' = \left[\frac{V_{xx} V_{yy} - V_{xy}^2}{V_{yy} u_x^2 + V_{xx} u_y^2 - 2V_{xy} u_x u_y} \right]^{1/2}.$$

The three-dimensional decay distance was obtained from l' using the relation $l = l'/\sin\theta$, where θ is the polar angle of the charm-meson flight direction. The proper decay time t and its error δt are then $t \pm \delta t = (l \pm \delta l) cM/p$ where M and p are, respectively, the mass and momentum of the charm meson.

We used the resulting list of measured decay times and errors and a maximum-likelihood method to obtain the most probable value for the lifetime of the charm particle. The likelihood function includes contributions from background as well as from signal. The signal was represented by the convolution of an error distribution whose shape was determined empirically from the measured events and an exponential decay function. The background decay time was represented by a similar error distribution with a mean value offset from zero. A scaling factor in the magnitude of the error values was also allowed. Decays of charm particles which are themselves decay products of B mesons were corrected for on a statistical basis. See Appendix A for a more complete discussion of the likelihood function.

A. D^0

The proper-decay-time distribution for the 55 events of the sample with $z_{D^*} \geq 0.4$ is shown in Fig. 20(a). Since the background population was so small, the cut on Δ was loosened to give 21 events with which to evaluate the apparent lifetime of the background under the D^0 peak. The apparent-decay-time distribution of these events is shown in Fig. 20(b). Two different methods of modeling the background-error distribution were tried in the maximum-likelihood fit. (See Appendix A.) One method employed a simple Gaussian using the error evaluated from the vertex fits scaled by a factor R' . The second

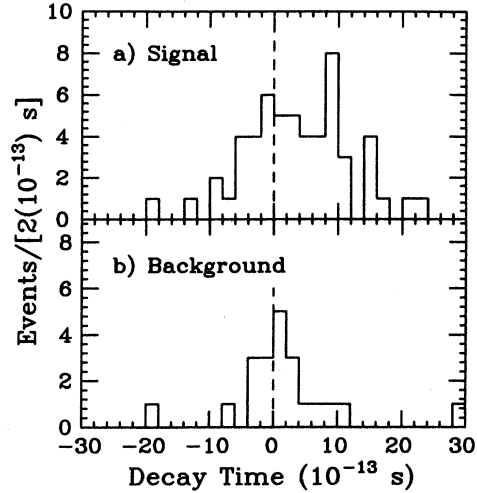


FIG. 20. (a) The proper-decay-time distribution for the D^0 mesons coming from D^{*+} mesons with $z_{D^*} \geq 0.4$. (b) The apparent-decay-time distribution of the increased sample of events in the background mass ranges $1.70 \leq M_{K\pi} \leq 1.80 \text{ GeV}/c^2$ and $1.93 \leq M_{K\pi} \leq 2.05 \text{ GeV}/c^2$ in the same range of z_{D^*} .

method utilized a weighted sum of two Gaussians one of which used the vertex-fit errors while the other used those errors scaled by a factor $R > 1$. The relative weights of the two Gaussians and the value R were adjusted to give the best fit to the background-decay-time distribution. The apparent background lifetime was found to be $(0.7 \pm 1.2) \times 10^{-13} \text{ s}$ using a relative weight of 0.3 for the second Gaussian and $R = 2.1$.

The B^0 decay contributes some D^0 decays to our sample which will have an apparently much longer lifetime. We corrected for this contribution by including in the likelihood function a term for a cascade decay. Refer to Appendix B for a discussion of the way the cascade decay is included in the probability-density function. The lifetime of the B^0 meson¹⁵ assumed for this cascade decay is $11.8 \times 10^{-13} \text{ s}$ (see Appendix C). The fraction of cascade decays in the sample was determined by generating a sample of Monte Carlo¹⁶ events with D^0 mesons coming

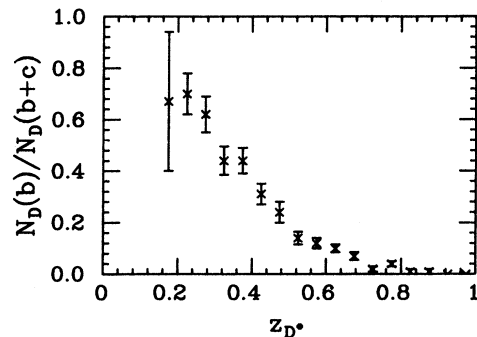


FIG. 21. The ratio of the number of D^0 mesons originating from b quarks to the total number of D^0 mesons as determined from the analysis of a Monte Carlo-generated event sample as a function of z_{D^*} .

both from direct c quarks and from b quarks by cascade. The fraction of those originating with b quarks is shown in Fig. 21. We used the functional form $0.34 \exp[(0.4 - z_{D^*})/0.15]$ to represent the fraction of cascade decays for $z_{D^*} \geq 0.4$.

The lifetime of the D^0 was obtained using the double-Gaussian shape, with the background and cascade-decay parameters discussed above. The best value for the D^0 lifetime was found to be $(4.4 \pm 1.0) \times 10^{-13}$ s.

The fraction of D^0 mesons from B^0 decay rises to about 50% for $z_{D^*} < 0.4$. We can therefore find the B^0 meson lifetime from the sample of data in this region of z_{D^*} . In fact if we attempt to measure the lifetime of the D^0 meson from this sample, without correcting for the B decay cascade, we obtain a result of $(12.1^{+7.6}_{-4.8}) \times 10^{-13}$ s. This is sufficiently different from the D^0 lifetime to suggest that there are noticeable B^0 contributions. The proper-decay-time distribution of the 22 events with $z_{D^*} < 0.4$ is shown in Fig. 22(a).

The evaluation of the apparent background lifetime was done in the same way as for the sample with $z_{D^*} \geq 0.4$. The statistics of the background sample was increased to 28 events by accepting events with $0.142 \leq \Delta \leq 0.149$ GeV/c^2 . The apparent-decay-time distribution of these events is shown in Fig. 22(b). The background lifetime for this sample was found to be $(4.9 \pm 2.4) \times 10^{-13}$ s with the same weight of the wider Gaussian as for $z_{D^*} \geq 0.4$ but with $R=3.7$. The same quantity evaluated only for the events with mass larger than the D^0 mass was $(3.6^{+3.2}_{-3.8}) \times 10^{-13}$ s, which is consistent with zero, whereas the apparent lifetime for the whole sample is 2 standard deviations from zero. As in the case of the D^+ , there is an indication that some of the events below the D^0 mass are true charm-particle events where a failure of tracking has spoiled the identification.

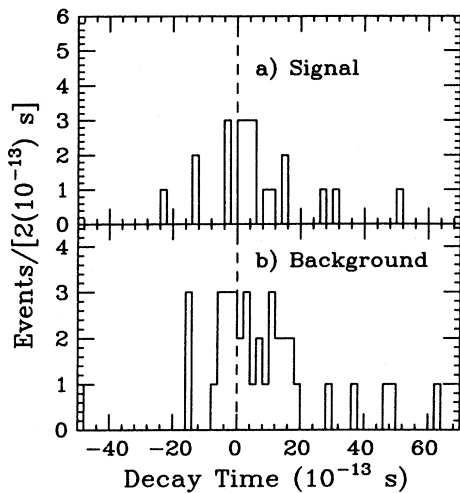


FIG. 22. (a) The proper-decay-time distribution of the D^0 mesons coming from D^{*+} mesons with $z_{D^*} < 0.4$. (b) The apparent-decay-time distribution of the increased sample of events in the background mass ranges $1.70 \leq M_{K\pi} \leq 1.80$ GeV/c^2 and $1.93 \leq M_{K\pi} \leq 2.05$ GeV/c^2 in the same range of z_{D^*} .

The value 3.6×10^{-13} s was chosen for the apparent background lifetime. The actual value used makes very little difference in the measurement of the B^0 lifetime.

The maximum-likelihood procedure with the single-Gaussian error distribution was employed to fit the decay-time distribution in Fig. 22(a) to obtain the best value of the B^0 lifetime. In so doing a value for the B^0 momentum was needed to relate path length to lifetime. The average value of the B^0 momentum that was used was 10.5 GeV/c , which was obtained from the fragmentation data of B mesons.¹³ The fraction of B^0 decays as a function of z_{D^*} was represented by the function $1.12 - 1.95z_{D^*}$ for $z_{D^*} < 0.4$. A fixed value of the D^0 lifetime of 4.3×10^{-13} s was used and the error multiplication factor R' was 1.26 to give the best fit. The result is $\tau_{B^0} = (8.2^{+5.7}_{-3.7}) \times 10^{-13}$ s. The statistical error on this quantity is large because of the limited number of events available. Nevertheless this is the first measurement of the lifetime of the B^0 meson as distinguished from the average b -quark lifetime. The measurement is subject to the assumptions enumerated in Appendix C.

B. D^+

The proper-decay-time distribution of the events with $1.83 \leq M_{K\pi\pi} \leq 1.89$ GeV/c^2 , the D^+ mass region, was calculated from the decay-distance distribution using the measured D^+ momentum. The proper-decay-time distribution is shown in Fig. 23(a). The background fraction in the D^+ mass region was determined by a fit to the mass distribution, shown in Fig. 13, to be $(79 \pm 3)\%$. In order to have a background sample that was free from D^+ contamination for determining the apparent lifetime of the background, the mass range $1.92 - 2.10$ GeV/c^2 was used. The vertex position of each of these events together with the beam position and the momentum of the three-

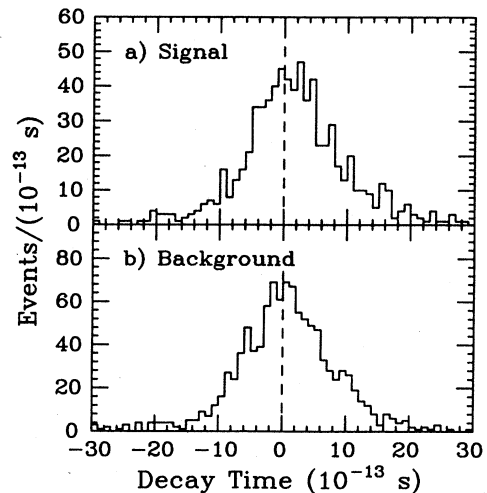


FIG. 23. (a) The proper-decay-time distribution for the D^+ events ($1.83 \leq M_{K\pi\pi} \leq 1.89$ GeV/c^2 in Fig. 13). (b) The apparent-decay-time distribution of the events in the background region $1.92 - 2.10$ GeV/c^2 of the same figure.

particle combination was used to determine an apparent-decay-time distribution. The apparent-decay-time distribution of the background is shown in Fig. 23(b).

Using the double-Gaussian method the best fit to the background-decay-time distribution was centered at a time of $(0.9 \pm 0.2) \times 10^{-13}$ s with a weight of 0.3 for the second Gaussian and $R=1.65$. The events in the D^+ mass region were fitted to an exponential-decay distribution convoluted with the same double Gaussian. The resulting best fit to the proper-time distribution is $\tau_{D^+} = (9.2_{-1.3}^{+1.7}) \times 10^{-13}$ s. The error includes the statistical error in the background determination.

C. D_s^+

The proper-decay-time distribution of the D_s^+ is shown in Fig. 24(a). Using the maximum-likelihood fit and the single-Gaussian error shape the lifetime was found to be $(3.1_{-2.0}^{+2.4}) \times 10^{-13}$ s with an R' factor of 1.3. The contribution of B -meson decay to the D_s^+ with $z_{D_s^+} > 0.4$ was taken to be 11% (see Appendix C), and the value of 11.8×10^{-13} s was used as the B lifetime.¹⁵ The fraction of the hadronic combinatorial background in the D_s^+ signal region was estimated to be 23%. The apparent-decay-time distribution of these events is shown in Fig. 24(b). The two background regions were combined since little difference was seen in their apparent lifetimes. The apparent lifetime of the 52 background events when fitted to a single-Gaussian shape was $(-0.2 \pm 1.0) \times 10^{-13}$ s, consistent with zero. A zero-background lifetime was therefore used in the overall fit.

VII. MONTE CARLO TEST RESULTS

A Monte Carlo study of our tracking procedures and lifetime analysis programs was carried out for each of the charm-meson decays. Hadronic events were generated

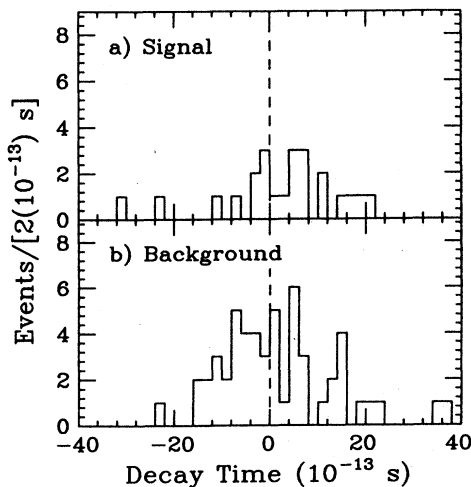


FIG. 24. (a) The proper-decay-time distribution of the D_s^+ mesons, the events in the mass range $1.94 \leq M_{\phi\pi} \leq 1.99$ GeV/c^2 in Fig. 16. (b) The apparent-decay-time distribution of the events in the background regions $1.70 \leq M_{\phi\pi} \leq 1.91$ GeV/c^2 and $2.02 \leq M_{\phi\pi} \leq 2.30$ GeV/c^2 .

by a Monte Carlo¹⁶ program which included D^0 , D^+ , and D_s^+ mesons decaying through all known channels with nominal lifetimes. In the case of the D_s^+ analysis smaller samples of events were also generated using several different lifetimes for the D_s^+ .

These Monte Carlo-generated tracks were propagated through the detector and used to generate hit distributions in all the tracking chambers of the detector. The effects of multiple scattering, energy loss, and conversion of photons were included in the simulation. The events were processed by our standard track finding and fitting routines to produce a data summary tape of reconstructed events.

For this Monte Carlo study the D^0 , D^+ , and D_s^+ events were selected using the same criteria as was used in the analysis of the data. In particular the same track-separation cuts in the vertex chamber and identical requirements on track quality were used. The tracking-error distributions and mass determinations were all consistent with the data.

A. D^0

A sample of e^+e^- events was generated which had at least one $D^* \rightarrow D^0 \rightarrow K\pi$ decay chain. The input lifetime was 4.4×10^{-13} s and the simulation included B -decay events. When the simulated events were analyzed in the same way as the data, a result of $(4.9 \pm 0.5) \times 10^{-13}$ s was obtained. Changing the event-selection criteria, such as the number of hits required in the vertex chamber, made no more than a change of $\pm 0.3 \times 10^{-13}$ s in the result.

B. D^+

The Monte Carlo-generated D^+ events were used to check for systematic errors introduced by the track-fitting programs and the track-quality cuts. The generated lifetime of the D^+ was 9.2×10^{-13} s. The analysis of these reconstructed events found a lifetime of $(8.1 \pm 1.3) \times 10^{-13}$ s which is consistent with the generated lifetime within the statistical errors.

C. D_s^+

Three sets of hadronic events were produced using the Monte Carlo program with lifetimes of the D_s^+ specified to be $(0.0, 2.0, \text{ and } 10.0) \times 10^{-13}$ s. The same cuts and track-quality requirements were placed on these sets of events as for the events described above. The resulting lifetimes were found to be $(-0.1 \pm 0.06, 3.0 \pm 0.7, 8.7 \pm 1.1) \times 10^{-13}$ s. Within these statistical errors no strong bias was observed in the lifetime determination.

VIII. RESULTS AND CONCLUSIONS

This section summarizes the measurements reported in this paper including estimates of the associated systematic errors as well as the statistical error. Some contributions to the systematic error affect all three decays in approximately the same way. These contributions, which are relatively small, arise from uncertainties in the tracking and vertex-fitting procedures and the determination

of the beam size and position. The estimate of the magnitude of these systematic errors is 0.3×10^{-13} s.

A. D^0

The following sources of systematic error in the determination of the lifetime of the D^0 meson have been investigated.

(i) The background is small so that uncertainty in the background fraction and the lifetime of the background contribute a small amount to the systematic error. If these quantities are changed by 1 standard deviation, the lifetime shifts by 0.1×10^{-13} s.

(ii) The result of the fit to the decay-time distribution using the single- and double-Gaussian error functions was the same but if the width scale factor R or R' was arbitrarily increased by 10% the lifetime shifted by 0.1×10^{-13} s.

(iii) The average fraction of D^0 mesons coming from B^0 mesons for $z_{D^*} \geq 0.4$ is estimated to be 10% according to the Monte Carlo study. If this number is changed to 15%, the lifetime is shifted by -0.2×10^{-13} s.

The sum in quadrature of these contributions, plus the uncertainties implied by the variations in the Monte Carlo study of variations due to changes in the tracking criteria, yield a value of 0.6×10^{-13} s for the systematic error. The final lifetime value is

$$\tau_{D^0} = (4.4 \pm 1.0 \pm 0.6) \times 10^{-13} \text{ s}$$

based on 55 events with $D^0 \rightarrow K^- \pi^+$.

The systematic error which is most important for the determination of the B^0 lifetime is the one that arises from the uncertainty in the number of D^0 mesons which come from direct charm as opposed to those coming from B^0 mesons. If the number of D^0 mesons is increased by 40% the lifetime of the B^0 meson is shifted by 2.7×10^{-13} s.

The final result for the B^0 lifetime, under the assumption that the charged B does not contribute significantly to the D^{*+} decay mode and the other assumptions enumerated in Appendix C, is

$$\tau_{B^0} = (8.2^{+5.7}_{-3.7} \pm 2.7) \times 10^{-13} \text{ s}$$

based on 22 events in which $D^{*+} \rightarrow D^0 \rightarrow K^- \pi^+$ with $0.19 \leq z_{D^*} \leq 0.4$.

B. D^+

For the D^+ lifetime determination the background subtraction is very important. We have made a parametric study of the background-fitting routines using the nominal D^+ mass to determine the systematic error.

(i) Carrying out the maximum-likelihood fit with the single-Gaussian method instead of the two-Gaussian method shifts the lifetime determination by $+1.3 \times 10^{-13}$ s.

(ii) A shift of the central value of the background Gaussian from 0.9×10^{-13} s to 0.0×10^{-13} s shifts the lifetime by $+0.3 \times 10^{-13}$ s.

(iii) A $\pm 5\%$ systematic error is ascribed to the back-

ground fraction determination. This yields a lifetime error of $\pm 0.8 \times 10^{-13}$ s.

An alternate scheme of direct background subtraction was used for fitting the D^+ lifetime distribution. The result is consistent with that of the maximum-likelihood technique. Contamination from B -meson decay is negligible due to the high- z cut required for this D^+ sample. In addition, contributions from the decay $D^+ \rightarrow K^0 \pi$ have been studied and found to be insignificant for the tracking cuts that were imposed.

These errors are added in quadrature to yield an estimate of the total systematic error 1.6×10^{-13} s. The resulting lifetime is

$$\tau_{D^+} = (9.2^{+1.7}_{-1.3} \pm 1.6) \times 10^{-13} \text{ s}$$

based on 155 events with $D^+ \rightarrow K^- \pi^+ \pi^+$ above a background of 609 events.

C. D_s^+

We have studied the following possible sources of systematic error.

(i) For the estimated uncertainty of 20% in the fraction of the hadronic combinatorial background, the corresponding lifetime change was 0.2×10^{-13} s.

(ii) Changing the hadronic combinatorial background lifetime by the amount of 1.0×10^{-13} s yielded a change in the lifetime of 0.2×10^{-13} s.

(iii) A 30% change in the estimated fraction of $B \rightarrow D_s^+$ decays changes the lifetime by 0.2×10^{-13} s.

The D_s^+ meson lifetime including the systematic error is

$$\tau_{D_s^+} = (3.1^{+2.4}_{-2.0} \pm 0.5) \times 10^{-13} \text{ s},$$

based on a sample of 23 $D_s^+ \rightarrow \phi + \pi^+$ decays.

D. Comparison with other experimental results

We have previously referred to some of the most important recent measurements of charmed-meson lifetimes⁵⁻⁸ and to a recent review of these measurements.² This recent review attempts to arrive at an overall average value for each lifetime taking into account both the quoted statistical and systematic errors. Each of the three lifetime averages depends most strongly, however, on the results of Ref. 7. These average values are $\tau_{D^0} = (4.27 \pm 0.10) \times 10^{-13}$ s, $\tau_{D^+} = (10.45^{+0.31}_{-0.29}) \times 10^{-13}$ s, and $\tau_{D_s^+} = (4.31^{+0.36}_{-0.32}) \times 10^{-13}$ s. Our measurements are clearly in agreement with them.

ACKNOWLEDGMENTS

This work was supported in part by the U.S. Department of Energy under Contracts Nos. W-31-109-ENG-38, DE-AC02-76ER01112, DE-AC76SF000998, DE-AC02-76ER01428, and DE-AC02-84ER0125. This experiment was made possible by the support provided by the PEP staff, the SLAC cryogenic support group, and the technical staffs of the collaborating institutions.

APPENDIX A: THE LIKELIHOOD FUNCTION

The likelihood function for several events is the product of the probability-density functions P_n evaluated at each measured value of the distributed variable. The quantity

$$\ln L = \sum_{n=1}^m P_n(x, y, z, \dots, t_n)$$

was evaluated for each set of parameters x, y, z, \dots and the set with the maximum value of $\ln L$ was chosen as the most probable set. The most probable errors in the parameters are obtained by generating the contour in the multiparameter space corresponding to a change in $\ln L$ of 0.5.

It is necessary to determine a mathematical form for the probability-density functions which describe the measured distributions. In the case that the lifetime is small compared with the normally distributed measurement error, the probability-density function may be approximated by a translated Gaussian

$$G(\sigma, t') \equiv (2\pi)^{-1/2} \sigma^{-1} \exp \left[-\frac{(t-t')^2}{2\sigma^2} \right],$$

where t' is the offset of the distribution from zero and σ is the calculated error in the variable t . This function is appropriate for the background events which have small apparent lifetimes.

The probability-density function appropriate for the fitting of the decay-time distributions is the convolution of an exponential distribution with the distribution representing the experimental resolution. The probability-density function for the exponential distribution is

$$E(\tau) = \frac{1}{\tau} \exp \left[-\frac{t}{\tau} \right]$$

and the convolution of a Gaussian and an exponential is

$$\begin{aligned} E(\tau) \otimes G(\sigma) &= \frac{(2\pi)^{-1/2}}{\sigma\tau} \int_{-\infty}^{t'} \exp \left[-\frac{t^2}{2\sigma^2} \right] \exp \left[-\frac{t-t'}{\tau} \right] dt \\ &= \frac{1}{2\tau} \exp \left[\frac{\sigma^2}{2\tau^2} - \frac{t'}{\tau} \right] \operatorname{erfc} \left[\frac{1}{\sqrt{2}} \left[\frac{\sigma}{\tau} - \frac{t'}{\sigma} \right] \right], \end{aligned}$$

where erfc is the complementary error function

$$\operatorname{erfc}(t) \equiv \frac{2}{\sqrt{\pi}} \int_t^{\infty} \exp(-x^2) dx.$$

APPENDIX B: THE PROBABILITY-DENSITY FUNCTION FOR CASCADE DECAY

The probability-density function for a cascade decay, such as $B \rightarrow D \rightarrow X$, is the convolution of a Gaussian with the convolution of two exponential distributions. The latter convolution is

$$\begin{aligned} E(\tau_1) \otimes E(\tau_2) &\equiv \frac{1}{\tau_1\tau_2} \int_0^{t'} \exp \left[-\frac{t}{\tau_1} \right] \exp \left[-\frac{t-t'}{\tau_2} \right] dt \\ &= \frac{1}{\tau_2 - \tau_1} \left[\exp \left[-\frac{t'}{\tau_2} \right] - \exp \left[-\frac{t'}{\tau_1} \right] \right] \\ &= \frac{\tau_1 E(\tau_1) - \tau_2 E(\tau_2)}{\tau_1 - \tau_2}. \end{aligned}$$

Thus

$$G(\sigma) \otimes E(\tau_1) \otimes E(\tau_2) = \frac{\tau_1 E(\tau_1) \otimes G(\sigma) - \tau_2 E(\tau_2) \otimes G(\sigma)}{\tau_1 - \tau_2}.$$

In the cascade decay a method is needed to partition the measured decay distance between the two decaying particles. The momentum of the final decay products of the D meson is measured whereas the momentum of the B meson must be assigned a value determined by other means. The partition must minimize the error arising from the unknown B -decay point. The composite measured decay length was apportioned to the B and D parts of the cascade decay according to their average decay lengths. Thus the adjusted decay time for the i th event for use in the cascade-decay-probability density function was

$$t_c^i = (F_B \langle l_B \rangle + F_D \langle l_D \rangle) \left[\frac{l_m^i}{\langle l_B \rangle + \langle l_D \rangle} \right],$$

where $F_B = M_{Bc} / \langle p_B \rangle$ is the length-to-time conversion factor for the B meson, $F_D = M_{Dc} / p_D^i$ is the same for the D meson, l_m^i is the measured distance, and $\langle \rangle$ indicates the average value. The conversion from the decay time of a simple D -meson decay to the cascade decay time can be simply expressed as

$$t_c^i = \frac{S}{S - T^i} t^i,$$

where $t^i = F_D^i l_m^i$, $S = 1 + \tau_D / \tau_B$, and $T^i = 1 - F_D^i / F_B$. There is a small error, in addition to error in t^i , in this estimate because average values have been used in place of true values for the B lifetime, the D lifetime, and the B momentum.

APPENDIX C: B-MESON DECAYS TO CHARM MESONS

A fraction of all of the charm particles produced in e^+e^- collisions with 29-GeV center-of-mass energy will arise from the decay of B mesons. Such mesons have a longer lifetime than the charm particles. In addition we cannot distinguish the charm particles which arise from B mesons from those that do not. There are cascades of two successive decays leading to apparent decay lengths that are much longer than those expected from a single charm-particle decay.

1. Compensating for cascade decays in the measurement of charm-particle lifetimes

The average b -quark lifetime has been measured fairly precisely but the lifetimes of the individual B mesons are

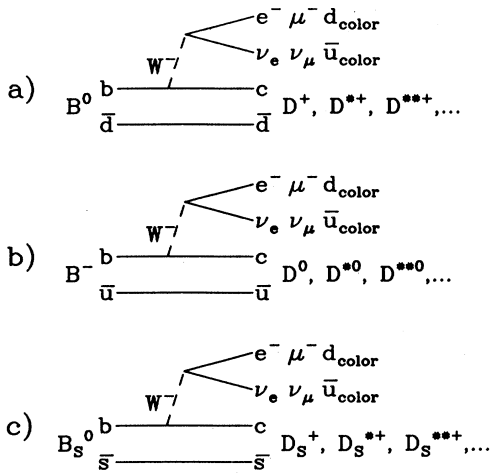


FIG. 25. Some spectator-model diagrams for the decay of (a) the B^0 meson, (b) the B^- meson, and (c) the B_s^0 meson.

not known. Nevertheless, in the measurement of the D^0 meson lifetime the D^{*+} mesons which come from b quarks come primarily from the B^0 meson while in the measurement of the D_s^+ lifetime most of the D_s^+ mesons which come from b quarks come from B_s^0 mesons. Fortunately, in both of these cases the correction for B -decay contamination is $\lesssim 10\%$.

The spectator diagram in Fig. 25 illustrates typical B -meson decays. (The B_c^- has not yet been observed and is probably produced much less frequently than the others so that it has been omitted.) The situation is very similar to that of the charm mesons but now the b quark is even heavier and the spectator assumption is even more appropriate. In the case of the D mesons there is a lifetime difference between the D^0 and D_s^+ mesons on the one hand and the D^+ meson on the other. Theoretical calculations suggest, however, that the effects which produce the lifetime difference between D mesons are smaller in the case of B mesons.¹⁷ Experimentally the 90% confidence limits $0.44 < \tau_{B^0}/\tau_{B^+} < 2.05$ have been obtained.¹⁸

The fraction of D_s^+ mesons which originate from B decay was obtained from the measured branching fraction of B to D_s^+ on the $\Upsilon(4s)$ resonance,¹⁵ which is 0.125 ± 0.034 , and the calculated branching fraction¹⁹ of the B_s^0 to D_s^+ of $0.86_{-0.13}^{+0.08}$. Assuming that B^0 and B^- are produced in equal numbers and 15% of the total number of B mesons are B_s^0 , the average decay fraction of B mesons to D_s^+ is 0.14. Then assuming that four c quarks are produced for every b quark, and that 15% of

all D mesons are D_s^+ , the ratio of D_s^+ produced from B mesons to those produced from c quarks is found to be 0.23. The relative acceptance by the cut on $z_{D_s^+} > 0.4$ is 0.53 so that, in our data, the fraction of D_s^+ coming from B decay is 0.11.

2. Extracting the B^0 lifetime from D^{*+} decays at low values of z_{D^*}

To measure the B^0 -meson lifetime from the decay of D^{*+} mesons at small values of z_{D^*} , it is necessary to show that a significant fraction of D^{*+} mesons actually come from B^0 mesons.

At the $q\bar{q}$ production vertex the ratio of $b\bar{b}$ production to $c\bar{c}$ production is 1 to 4. The decay of b to c dominates over b to u and the c quark decays predominantly to the D^* meson.²⁰ The D^* mesons from B decay have a much softer momentum spectrum than the c quarks produced at the $\gamma q\bar{q}$ vertex because a considerable fraction of the energy of the B is carried off by the W^- (see Fig. 25). The results of a Monte Carlo¹⁶ study of all these effects, together with the special geometric cuts imposed by the detector, are shown in Fig. 21. For z_{D^*} less than 0.4 there are about equal numbers of D^{*+} mesons from B decay and from the primary production. The threshold for the detection of D^{*+} mesons is at $z=0.19$ because of a lower limit on the acceptable momentum of the pion from D^{*+} decay.

It is expected, from the quark diagrams in Fig. 25, that charged D^{*+} mesons come from B^0 mesons. Some D^{*+} mesons, however, will come from B^- mesons when the B^- decays to $D^{*+}\pi^-$ plus the W^- decay products. The $D^{*+}\pi^-$ may or may not be in the resonant state D^{**0} (Ref. 21). The branching ratio of B^- decay to D^{*+} through this mechanism is not known at this time, although it is probably not large. As emphasized above the B^0 semileptonic decay rate is nearly saturated by decays to D^+ and D^{*+} states, and the B^- semileptonic decay would occur with the same relative probability to these states. In particular, if there is a small amount of D^{**+} in B^0 decay there should also be a correspondingly small amount of D^{**0} in B^- decay. Then if τ_{B^0} is short enough that the D^+ and D^{*+} completely saturate the semileptonic branching ratio, the $D^{**0} \rightarrow D^{*+}$ decay mode of B^- is insignificant. In any case there is no correction to τ_{B^0} if τ_{B^0} is the same as the average B lifetime. For other values of τ_{B^0} there is an additional uncertainty because of the uncertainty in the amount of $B^- \rightarrow D^{*+}X$.

*Present address: CRN Div. de Hautes Energies, F-67037 Strasbourg, France.

†Present address: Stanford Linear Accelerator Center, Stanford, California.

‡Present address: National Instituut voor Kernfysica en Hoge-Energiefysica, 1009 DB Amsterdam, Noord-Holland, The

Netherlands.

§Present address: Bell Laboratories, Murray Hill, New Jersey 07974.

**Present address: University of Wisconsin, Madison, Wisconsin 53706.

††Present address: Ohio State University, Columbus, Ohio

- 43210.
- ††Present address: Virginia Polytechnic Institute, Blacksburg, Virginia 24061.
- ¹M. Kobayashi and T. Maskawa, *Prog. Theor. Phys.* **49**, 652 (1973).
- ²D. Hitlin, in *Lepton and Photon Interactions*, proceedings of the International Symposium on Lepton and Photon Interactions at High Energies, Hamburg, West Germany, 1987, edited by R. Rueckl and W. Bartel [*Nucl. Phys. B, Proc. Suppl.* **3**, (1988)].
- ³M. Bauer, B. Stech, and M. Wirbel, *Z. Phys. C* **34**, 103 (1987); B. Yu. Blok and M. A. Shifman, *Yad. Fiz.* **45**, 211 (1987) [*Sov. J. Nucl. Phys.* **45**, 135 (1987)]; **45**, 478 (1987) [**45**, 301 (1987)]; **45**, 841 (1987) [**45**, 522 (1987)]; A. J. Buras, J.-M. Gerard, and R. Rückl, *Nucl. Phys.* **B268**, 16 (1986); L.-L. Chau and H.-Y. Cheng, *Phys. Rev. D* **36**, 137 (1987); A. N. Kamal and R. Sinha, *J. Phys. G* **13**, L137 (1987); A. N. Kamal and R. C. Verma, *Phys. Rev. D* **35**, 3515 (1987); A. N. Kamal, *J. Phys. G* **12**, L43 (1986); *Phys. Rev. D* **33**, 1344 (1986).
- ⁴C. Jung *et al.*, *Phys. Rev. Lett.* **56**, 1775 (1986).
- ⁵H. Yamamoto *et al.*, *Phys. Rev. D* **32**, 2901 (1985); L. Gladney *et al.*, *ibid.* **34**, 2601 (1986); M. Althoff *et al.*, *Z. Phys. C* **32**, 343 (1986); S. R. Wagner *et al.*, *Phys. Rev. D* **36**, 2850 (1987); W. Braunschweig *et al.*, *Z. Phys. C* **35**, 317 (1987); S. E. Csorna *et al.*, *Phys. Lett. B* **191**, 318 (1987).
- ⁶H. Becker *et al.*, *Phys. Lett. B* **184**, 277 (1987); H. Palka *et al.*, *Z. Phys. C* **35**, 151 (1987).
- ⁷J. R. Raab *et al.*, *Phys. Rev. D* **37**, 2391 (1988).
- ⁸M. Aguilar-Benitez *et al.*, *Z. Phys. C* **34**, 143 (1987).
- ⁹D. Bender *et al.*, *Phys. Rev. D* **30**, 515 (1984).
- ¹⁰D. Rubin *et al.*, *Nucl. Instrum. Methods* **203**, 119 (1982).
- ¹¹P. Baringer, C. Jung, H. O. Ogren, and D. R. Rust, *Nucl. Instrum. Methods* **A254**, 542 (1987).
- ¹²J. S. Loos *et al.*, *Nucl. Instrum. Methods* **A249**, 185 (1986).
- ¹³M. Aguilar-Benitez *et al.*, *Phys. Lett.* **170B**, 1 (1986).
- ¹⁴J. Jaros *et al.*, *Phys. Rev. Lett.* **51**, 955 (1983); also see René Ong and Keith Riles, SLAC MARK II/SLC Note No. 166, 1986 (unpublished).
- ¹⁵W. Schmidt-Parzefall, in *Lepton and Photon Interactions* (Ref. 2).
- ¹⁶Our Monte Carlo generator was a modified form of the Lund Monte Carlo version 5.3.
- ¹⁷M. B. Voloshin and M. A. Shifman, *Zh. Eksp. Teor. Fiz.* **91**, 1180 (1986) [*JETP* **64**, 698 (1986)]; M. B. Voloshin, N. G. Ural'tsev, V. A. Khoze, and M. A. Shifman, *Yad. Fiz.* **46**, 181 (1987) [*Sov. J. Nucl. Phys.* **46**, 112 (1987)].
- ¹⁸A. Bean *et al.*, *Phys. Rev. Lett.* **58**, 183 (1987).
- ¹⁹Mahiko Suzuki, *Phys. Rev. D* **31**, 1158 (1985).
- ²⁰D. Bortoletto *et al.*, *Phys. Rev. D* **35**, 19 (1987); **37**, 1719 (1988).
- ²¹H. Albrecht *et al.*, *Phys. Rev. Lett.* **56**, 549 (1986).